RESEARCH ARTICLE

NEURODEVELOPMENT

Astrocytes close the mouse critical period for visual plasticity

Jérôme Ribot[1]†, Rachel Breton[1,2,3]†, Charles-Félix Calvo[1], Julien Moulard[1,4], Pascal Ezan[1], Jonathan Zapata[1], Kevin Samama[1], Matthieu Moreau[5], Alexis-Pierre Bemelmans[6], Valentin Sabatet[7], Florent Dingli[7], Damarys Loew[7], Chantal Milleret[1], Pierre Billuart[5], Glenn Dallérac[1]‡§, Nathalie Rouach[1]*§

Brain postnatal development is characterized by critical periods of experience-dependent remodeling of neuronal circuits. Failure to end these periods results in neurodevelopmental disorders. The cellular processes defining critical-period timing remain unclear. Here, we show that in the mouse visual cortex, astrocytes control critical-period closure. We uncover the underlying pathway, which involves astrocytic regulation of the extracellular matrix, allowing interneuron maturation. Unconventional astrocyte connexin signaling hinders expression of extracellular matrix–degrading enzyme matrix metalloproteinase 9 (MMP9) through RhoA–guanosine triphosphatase activation. Thus, astrocytes not only influence the activity of single synapses but also are key elements in the experience-dependent wiring of brain circuits.

During the first weeks of mouse life, massive synaptogenesis is followed by the shaping of synaptic circuits (*1*). Astrocyte processes, as structural and signaling partners of individual synapses, regulate neurotransmission and plasticity (*2*, *3*). Astrocytes are also implicated in the tuning and synchronization of neuronal network activities and influence cognitive functions such as memory formation (*4*). However, whether astrocytes take part in the wiring of the neuronal circuitry that occurs during critical periods of mouse postnatal development remains to be investigated. In the visual cortex, experience shapes synaptic circuits during a period of enhanced plasticity that follows eye opening (*5*, *6*). Introducing immature astrocytes in adult cats reopens a period of high plasticity, reminiscent of the critical period (*7*). However, whether and how the maturation of astrocytes actually controls critical-period closure remain unclear.

Immature astrocytes favor plasticity

We first investigated the ability of immature astrocytes to promote visual cortex plasticity in adult mice. To this end, we cultured and labeled, using lentivirus PGK-GFP (phosphoglycerate kinase–green fluorescent protein), immature astrocytes from the cortex of P1 to P3 (postnatal day 1 to 3) mice—which we characterized using immunolabeling (fig. S1)—and implanted them 10 days later in the primary visual cortex (V1) of adult mice (P100), in which the critical period is closed (Fig. 1A). Two weeks after the graft, we tested mice for ocular dominance (OD) plasticity—a form of plasticity typical of the critical period, where changes in visual inputs alter the natural dominance of the contralateral eye. To do so, we assessed visual cortex activity using optical imaging of intrinsic signals after 4 days of monocular deprivation (MD) (Fig. 1A). We found that mice engrafted with immature astrocytes displayed a high level of plasticity, unlike control mice subjected to MD with injection of culture medium or noninjected mice (Fig. 1B). Whereas in the wild-type (WT) mature visual cortex this plasticity is the result of an increase in the nondeprived eye response, in engrafted mice, it resulted from a reduction of the deprived eye response, which is typical of immature systems (*8*) (fig. S2). These data indicate that immature astrocytes reopen OD plasticity in adult mice.

To identify how immature astrocytes allow OD plasticity, we then investigated the molecular determinants of astrocyte maturation. Comparing gene expression of immature (P7) versus mature (P30) astrocytes using the transcriptome database for astrocytes during development (*9*) revealed ~200 genes that were differentially expressed with a fold-change >5 (table S1). Gene ontology analysis of enriched astrocyte gene groups identified a functional switch during maturation from cell division to cell communication, with the cell junction genes being the most represented (table S2 and fig. S3). Among these genes, *Gjb6*, encoding the astrocyte gap-junction channel subunit connexin 30 (Cx30), displayed one of the highest increases in expression (fold-change = 9; $P = 0.0274$; table S1). Accordingly, Cx30 regulates the structural maturation of hippocampal astrocytes during postnatal development (*10*). Together, these data led us to investigate the role of Cx30 in the astrocytic control of the critical period. To do so, we first assessed the regional and temporal expression of Cx30 in the mouse V1. Using immunohistochemistry, we found that Cx30 is enriched in layer 4 (Fig. 1C), the main V1 input layer, identified by wisteria floribunda agglutinin (WFA)—a marker of perineuronal nets important for the time course of the critical period (*11*). This enrichment correlates with a high density of astrocytes labeled in the Aldh1l1-GFP mice (Fig. 1C). Moreover, the Cx30 protein level in V1 increased from P10 to P50, as shown by Western blot (Fig. 1D), reaching its maximum when the critical period ends, which suggests that it may contribute to its closure. If so, reopening a phase of high plasticity should be associated with a down-regulation of Cx30. As a period of dark exposure (DE) can reinstate visual cortex plasticity during adulthood after closure of the critical period (*12*, *13*), we placed WT adult mice (P50) in the dark for 4 days and quantified V1 Cx30 levels. We found that this manipulation reduced Cx30 protein levels (~−70%) (Fig. 1E). We also found that 4 days of DE induced V1 plasticity, as indicated by the change in OD index (Fig. 1F). Thus, the drop in Cx30 expression correlated with plasticity induction.

Astrocytic Cx30 closes the critical period

We then investigated whether Cx30 inhibits OD plasticity. To do so, we first generated a knockdown mouse line for astrocytic Cx30 (KD), where Cx30 expression is decreased in V1 astrocytes by ~80% (fig. S4). In these mice, electroretinograms were unaltered, suggesting normal retinal functions (fig. S5). We found that OD plasticity peaked at P28 in WT

[1]Center for Interdisciplinary Research in Biology, Collège de France, CNRS UMR 7241, INSERM U1050, Labex Memolife, PSL Research University, Paris, France. [2]Doctoral School N°568, Paris Saclay University, PSL Research University, Le Kremlin Bicetre, France. [3]Université Paris-Saclay, CNRS, Institut des neurosciences Paris-Saclay, Gif-sur-Yvette, France. [4]Doctoral School N°158, Sorbonne University, Paris, France. [5]Université de Paris, Institute of Psychiatry and Neuroscience of Paris (IPNP), INSERM U1266, Genetic and Development of Cerebral Cortex Laboratory, GHU Paris Psychiatrie et Neurosciences, Hôpital Saint Anne, Paris, France. [6]Commissariat à l'Energie Atomique et aux Energies Alternatives (CEA), Département de la Recherche Fondamentale, Institut de biologie François Jacob, MIRCen, and CNRS UMR 9199, Université Paris-Saclay, Neurodegenerative Diseases Laboratory, Fontenay-aux-Roses, France. [7]Institut Curie, PSL Research University, Mass Spectrometry and Proteomics Laboratory, Paris, France.
***Corresponding author. Email: nathalie.rouach@college-de-france.fr**
†These authors contributed equally to this work.
‡Present address: Université Paris-Saclay, CNRS, Institut des neurosciences Paris-Saclay, Gif-sur-Yvette, France.
§These authors contributed equally to this work.

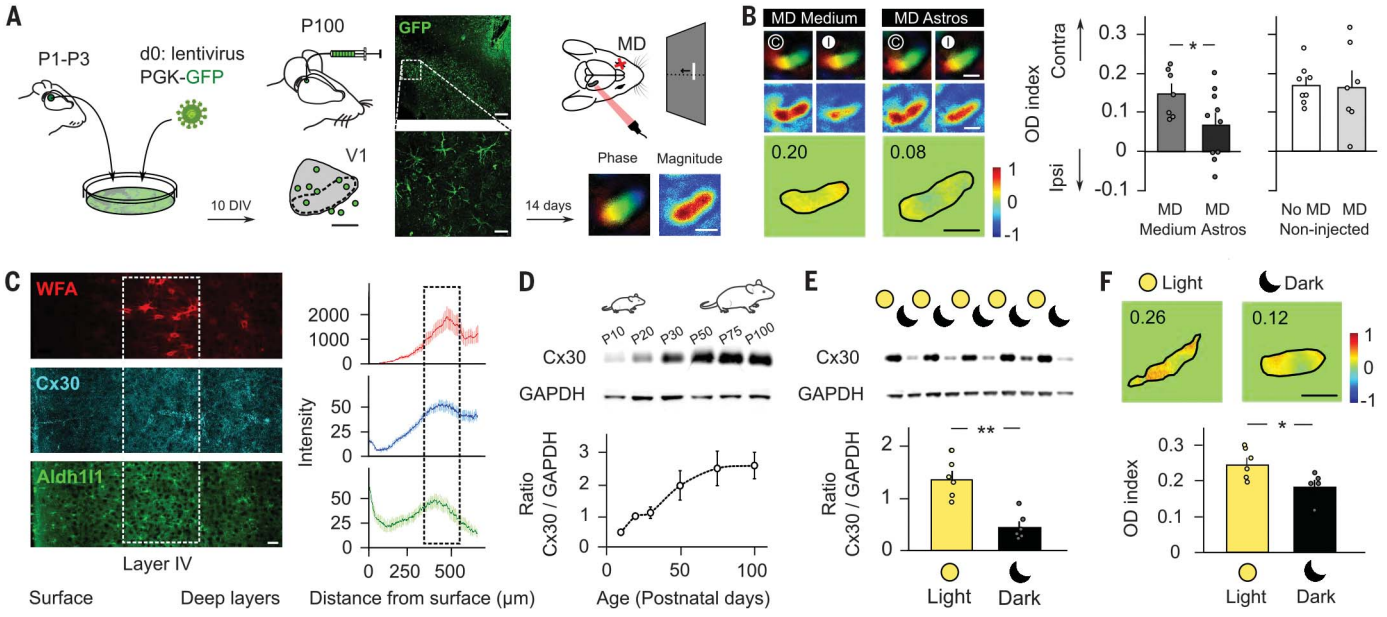

Fig. 1. Immature astrocytes favor cortical plasticity. (**A**) Immature astrocytes from P1 to P3 mice were transduced with PGK-GFP lentivirus, cultured for 10 days in vitro (DIV), and injected in the right V1 area of adult mice (P100), as shown on the schematic (green circles), where the dashed line represents the binocular zone. Scale bar, 1 mm. Confocal images of GFP-expressing astrocytes integrated in the mouse visual cortex 14 days after the injection are shown. Scale bars, 200 μm (top) and 20 μm (bottom). Intrinsic optical imaging was then conducted 14 days after the graft to record phase and magnitude retinotopic maps for each eye stimulation after 4 days of MD of the contralateral (left) eye. Scale bar, 1 mm. (**B**) These maps are shown in top panels for animals injected with control medium (medium MD; $n = 7$) or immature astrocytes (astro MD; $n = 10$). Contralateral (C) and ipsilateral (I) visual stimulations are indicated with a white (nondeprived eye) or black (deprived eye) circle. Bottom panels show the normalized OD map with average value inset. Mice injected with immature astrocytes showed a marked increase in OD plasticity compared with control mice injected with culture medium [$P = 0.043$, degree of freedom (DF) = 15, two-tailed t test], whereas no effect was observed in noninjected mice (no MD, $n = 8$; MD, $n = 7$; $P = 0.899$, DF = 13, two-tailed t test). (**C**) Representative immunostaining for WFA (top), Cx30 (middle), and Aldh1l1 (bottom) in V1 of P50 mouse (left panels) and corresponding quantification of spatial distributions across V1 layers (right panels; $n = 3$ mice). Scale bar, 50 μm. (**D** and **E**) Western blot analysis reveals changes in Cx30 levels in the visual cortex during development (D) [$n = 6$ per age; $P = 0.0001$, Kruskal-Wallis (KW) = 22.31)] and after 4 days of DE (E) ($n = 6$ per group; $P = 0.0022$, $U = 0$, Mann-Whitney test). GAPDH, glyceraldehyde 3-phosphate dehydrogenase. (**F**) Intrinsic optical imaging for light ($n = 6$) and dark ($n = 5$) exposed animals showing that DE decreased OD index ($P = 0.035$, DF = 9, two-tailed t test). Scale bar, 1 mm.

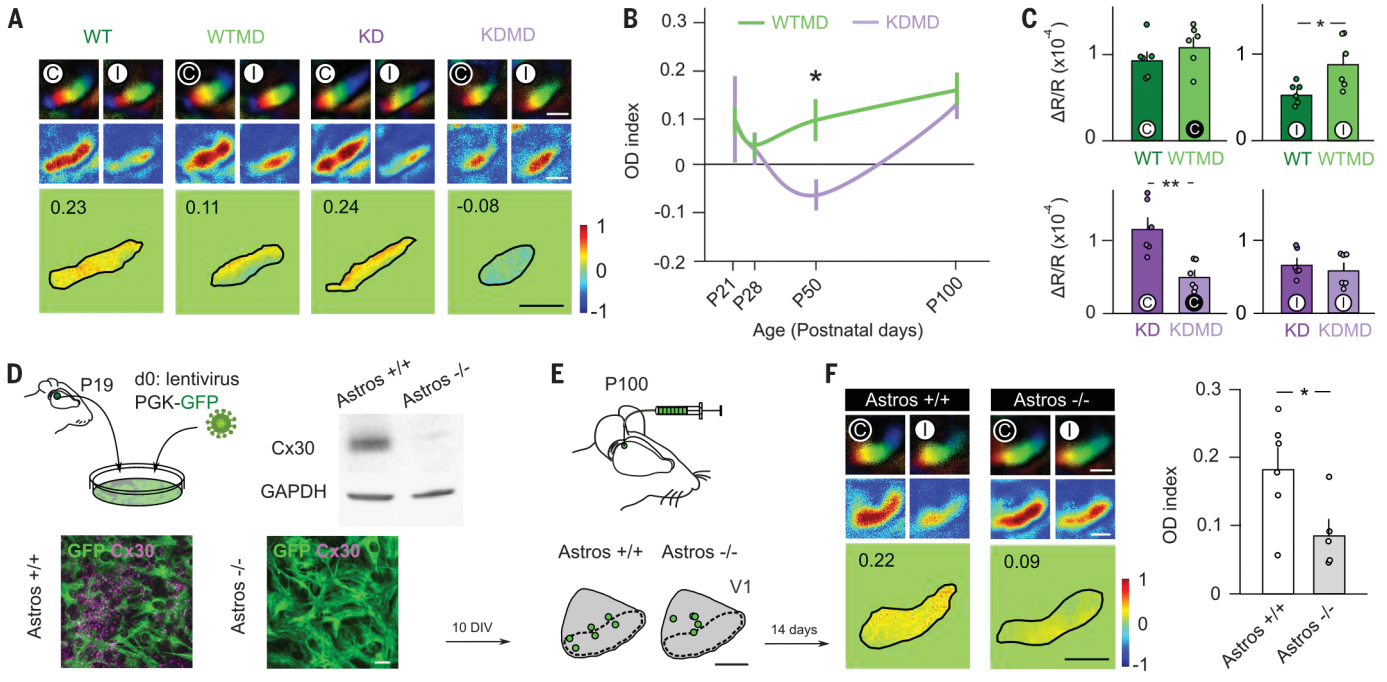

Fig. 2. Astrocytic Cx30 closes the critical period. (**A**) Functional maps in P50 WT and KD mice in control and MD conditions (WTMD and KDMD). Scale bar, 1 mm. (**B**) Developmental profile of OD index after MD in WT (P21, $n = 6$; P28, $n = 7$; P50, $n = 6$; and P100, $n = 7$) and KD mice (P21, $n = 3$; P28,

n = 8; P50, *n* = 6; and P100, *n* = 11), indicating a protracted and enhanced plasticity at P50 in KD mice [*P* = 0.0232, DF = 46, two-way analysis of variance (ANOVA) followed by Sidak post hoc test]. (**C**) Changes in response magnitude after MD in P50 mice results from an increased response to the nondeprived (white circle) eye (ipsilateral, I) stimulation in WT mice (*n* = 6 for WT and WTMD; *P* = 0.0411, *U* = 5, Mann Whitney test) and from a decreased response to the deprived (black circle) eye (contralateral, C) stimulation in KD mice (*n* = 6 for KD and KDMD; *P* = 0.0022, *U* = 0, Mann-Whitney test). (**D**) Mature astrocytes expressing or not expressing Cx30 were isolated from P19 WT (Astros +/+) or Cx30 constitutive knockout mice (Astros −/−), respectively, and were then transduced with PGK-GFP lentiviruses and cultured for 10 DIV. Western blots and immunostaining show expression of Cx30 in Astros +/+ but not in Astros −/−. Scale bar, 50 μm. (**E**) The cultured astrocytes were injected in adult mice (P100), as shown on the schematics (green circles). Scale bar, 1 mm. (**F**) Functional maps assessed 14 days after the graft show that OD plasticity after 4 days of MD is enhanced in mice injected with Astros −/− (*n* = 5) compared with mice injected with Astros +/+ (*n* = 6; *P* = 0.038, DF = 9, two-tailed *t* test). Scale bar, 1 mm.

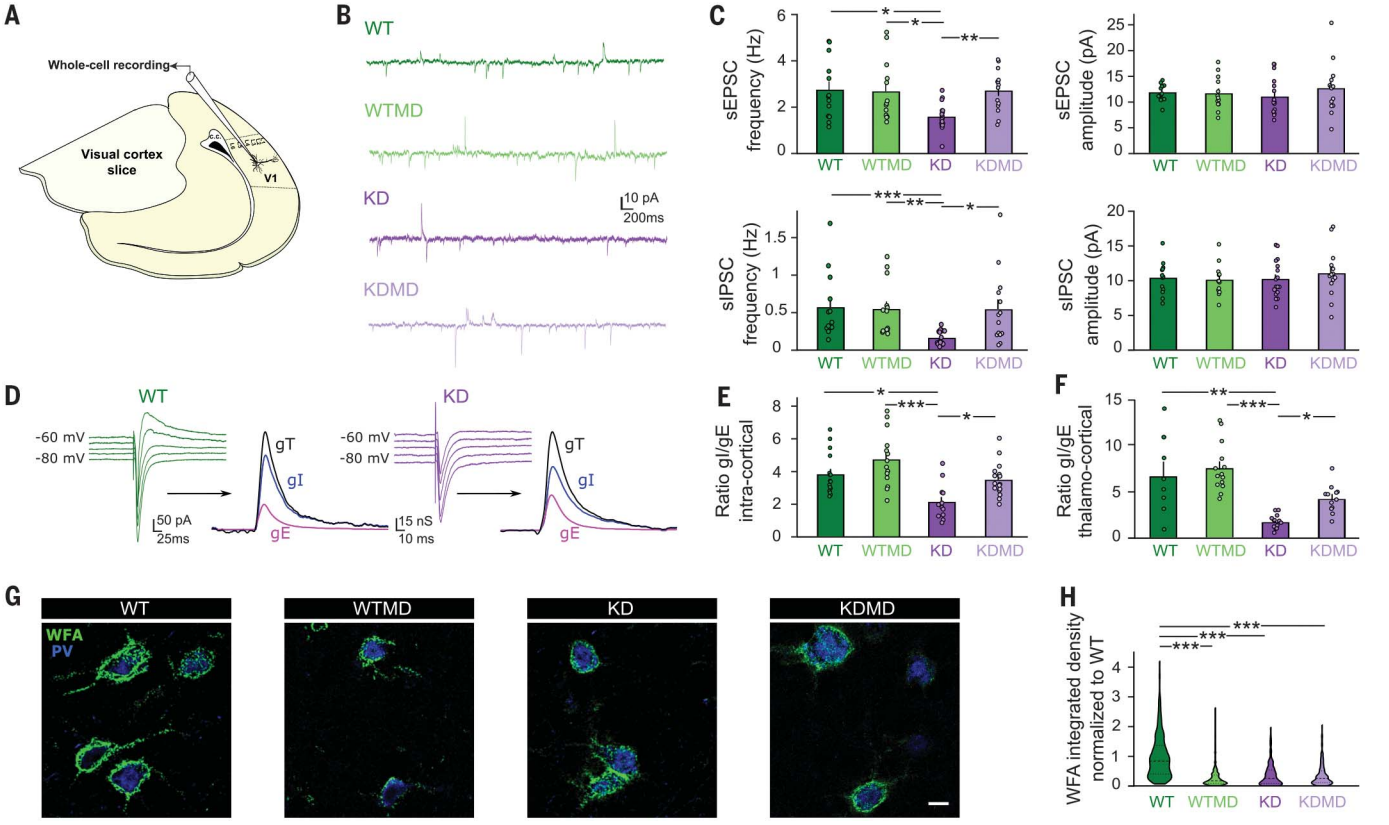

Fig. 3. Astrocytic Cx30 promotes the maturation of inhibitory circuits. (**A**) Schematic diagram depicting the brain slice from which V1 pyramidal neurons from layer 4 were recorded. (**B**) Example traces of sEPSCs (inward) and sIPSCs (outward). (**C**) Frequency, but not amplitude, of both sEPSCs and sIPSCs was decreased in KD (*n* = 17 cells; *P* = 0.0307 for sEPSCs and *P* = 0.009 for sIPSCs) compared with WT mice (*n* = 13 cells). MD induced no plasticity in WT mice (WTMD: *n* = 13 cells; *P* > 0.9999 for sEPSCs, *P* > 0.9999 for sIPSCs), whereas it potentiated both the sEPSCs and sIPSCs in KD mice (KDMD: *n* = 14 cells; *P* = 0.0084 for sEPSCs and *P* = 0.0227 for sIPSCs, Dunn's post hoc test after Kruskal-Wallis, KW = 13.61 for sEPSCs and KW = 20.04 for sIPSCs). (**D**) Example of evoked composite responses at increasing holding potentials allowing decomposition of the total conductance (gT) into excitatory (gE) and inhibitory (gI) conductances in WT and KD mice. (**E**) I/E ratio after intracortical stimulation was reduced in KD mice (*n* = 12 cells; *P* = 0.0143) compared with WT mice (*n* = 16 cells). MD induced no change in WT mice (WTMD: *n* = 14 cells; *P* = 0.78), whereas it increased the I/E ratio in KD mice (KDMD: *n* = 16 cells; *P* = 0.0498, Dunn's post hoc test after Kruskal-Wallis, KW = 19.53). (**F**) I/E ratio after thalamocortical stimulation was reduced in KD mice (*n* = 14 cells; *P* = 0.0029) compared with WT (*n* = 8 cells). MD induced no change in WT mice (WTMD: *n* = 14 cells; *P* > 0.9999), whereas it increased the I/E ratio in KD mice (KDMD: *n* = 12 cells; *P* = 0.0462, Dunn's post hoc test after Kruskal-Wallis, KW = 29.79). (**G** and **H**) WFA immunostaining (G) and violin plot (H) showing smaller PNN around PV interneurons in KD (*n* = 177 cells from 16 mice; *P* < 0.0001), WTMD (*n* = 171 cells from six mice; *P* < 0.0001), and KDMD mice (*n* = 238 cells from six mice; *P* < 0.0001) compared with WT mice (*n* = 295 cells from 19 mice) (Kruskal-Wallis, KW = 247.9, followed by Dunn's multiple comparisons post hoc).

mice. By contrast, this plasticity continued to increase in KD mice until P50, which indicates an impairment in the closure of the critical period (Fig. 2, A and B). Whereas in WT mice this plasticity was the result of an increase in the nondeprived eye response, in KD mice, it resulted from a reduction of the deprived eye response (Fig. 2C), which typically reflects changes occurring in mature and immature systems, respectively (*8*). These data thus indicate that Cx30 is required for proper maturation of the visual cortex. To further test whether the expression of Cx30 in mature astrocytes inhibits OD plasticity, we engrafted mature astocytes expressing or not expressing

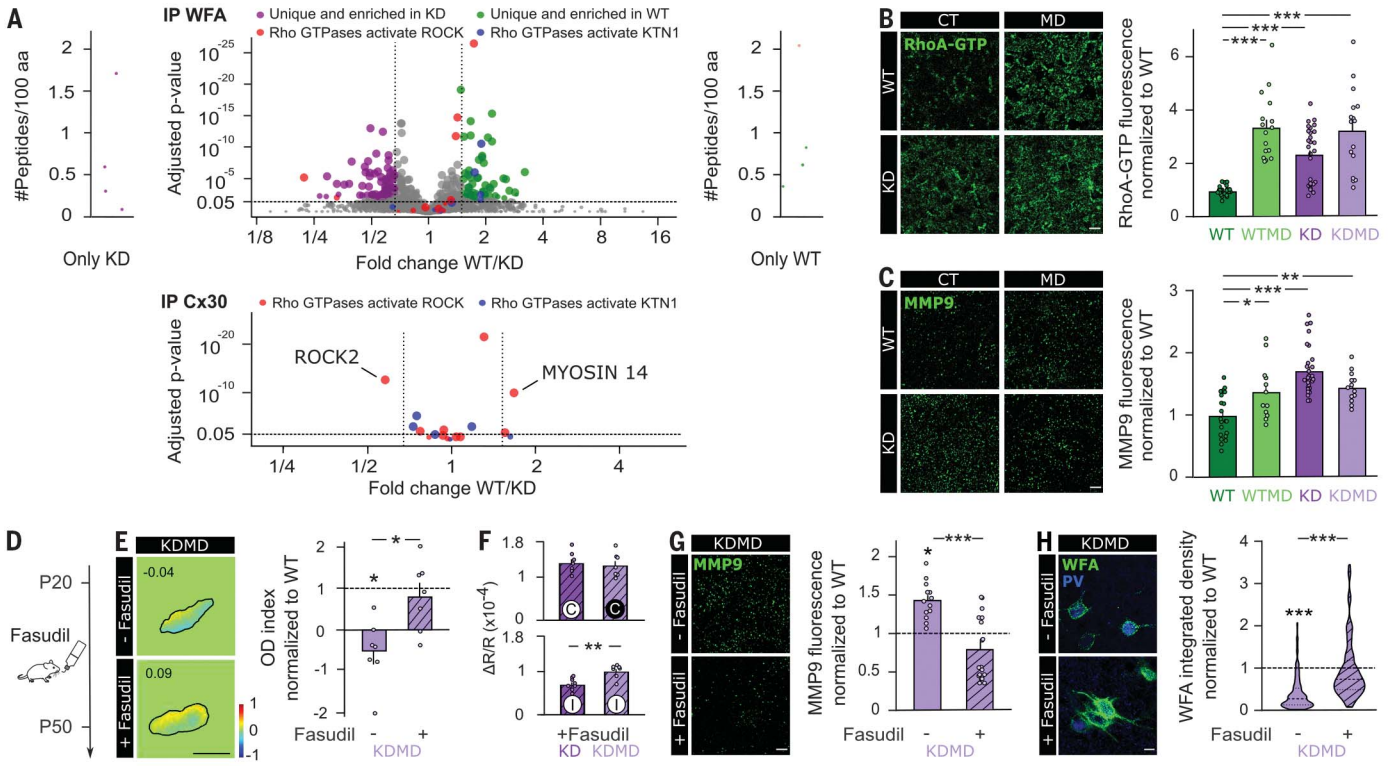

Fig. 4. Astrocytic Cx30 down-regulates the RhoA-MMP9 pathway involved in OD plasticity. (**A**) Identification of WFA and Cx30 binding partners by quantitative label-free mass spectrometry analysis. (Top) Volcano plot representing the 2096 quantified proteins enriched with biotinylated WFA lectin in KD and WT mice (n = 3). Proteins from the enriched pathways Rho-GTPase activate KTN1 (blue) and Rho-GTPase activate ROCK (red) are highlighted. (Bottom) Volcano plot analysis representing interactors of Cx30 from the Rho-GTPase activate KTN1 (blue) and Rho-GTPase activate ROCK (red) pathways. The fold-change in WT (n = 5) versus KD mice (n = 4) is shown with selected proteins (Rock2 and Myosin 14). Dashed vertical and horizontal lines show absolute fold-change of 1.5 and adjusted P value of ratio significance of 0.05, respectively. aa, amino acid. (**B**) Immunostaining for RhoA-GTP showed a marked increase in KD (n = 27; P = 0.0003), KDMD (n = 16; P < 0.0001), and WTMD mice (n = 16; P < 0.0001) compared with WT mice (n = 22) (fields of view from three mice per group) (Kruskal-Wallis, KW = 41.23, followed by Dunn's post hoc test). Scale bar, 10 μm. (**C**) Immunostaining for MMP9 shows a marked increase in KD mice (n = 28; P < 0.0001, DF = 71), KDMD (n = 13; P = 0.0059, DF = 71), and WTMD mice (n = 12; P = 0.0322, DF = 71) compared with WT mice (n = 22) [one-way ANOVA F(3.71) = 15.07 followed by Tukey's post hoc test]. Scale bar, 4 μm. (**D**) Diagram depicting the protocol for experimental treatment with fasudil. (**E** to **H**) Fasudil in KD mice after MD fully rescued WT OD plasticity (E), adult pattern of visual cortex responses to eye stimulation (F), MMP9 levels (G), and PNN extent (H). Contralateral (C) and ipsilateral (I) visual stimulations are indicated with a white (nondeprived eye) or black (deprived eye) circle. Scale bars, 1 mm (E), 4 μm (G), and 10 μm (H). Statistics for (E) OD index: KDMD, n = 6 mice; KDMD + fasudil, n = 7 mice; WTMD, n = 6 mice. P = 0.0343 between KDMD and KDMD + fasudil; P = 0.0215 between WTMD and KDMD; and P = 0.9357 between KDMD + fasudil and WTMD; ANOVA [F(2,16) = 5.534] followed by Tukey's post hoc test. (F) Signal amplitude of visual cortex responses: KD + fasudil, n = 7 mice; KDMD + fasudil, n = 7 mice. Contralateral eye (top): P = 0.7104, U = 21, Mann-Whitney test; ipsilateral eye (bottom): P = 0.0041, U = 3, Mann-Whitney test. (G) MMP9 levels: KDMD, n = 13; KDMD + fasudil, n = 18; WT, n = 22 from three mice (n represents the number of fields of view). P = 0.0001 between KDMD and KDMD + fasudil; P = 0.0124 between WT and KDMD; P = 0.349 between KDMD + fasudil and WT; Kruskal-Wallis (KW = 17.25) followed by Dunn's post hoc test. (H) PNN levels: KDMD, n = 238 PV cells from six mice; KDMD + fasudil, n = 105 PV cells from three mice; WT, n = 295 PV cells from 19 mice. P < 0.0001 between KDMD and KDMD + fasudil; P < 0.0001 between WT and KDMD; P > 0.9999 between WT and KDMD + fasudil; Kruskal-Wallis (KW = 164.7) followed by Dunn's post hoc test.

Cx30. To do so, we isolated astrocytes from P19 WT or constitutive Cx30 knockout mice, then cultured them for 10 days (fig. S6 and Fig. 2, D and E). We found that only the graft of mature astrocytes lacking Cx30 reopened OD plasticity in adult mice (Fig. 2F). Altogether, these data indicate that astrocytic Cx30 controls the timing of the critical-period closure.

Astrocytic Cx30 promotes maturation of inhibitory circuits

The temporal course of the visual cortex critical period is determined by the maturation of local inhibitory circuits controlling the excitation-inhibition (E/I) balance (*14*–*16*). To get insights on the physiological processes by which Cx30 closes the critical period, we measured changes in excitatory and inhibitory synaptic transmission after MD in pyramidal neurons from layer 4 of the visual cortex of WT and KD adult mice (P50) (Fig. 3A). The frequency, but not the amplitude, of both spontaneous excitatory and inhibitory postsynaptic currents (sEPSCs and sIPSCs) was reduced in KD mice compared with WT mice (Fig. 3, B and C), with sIPSCs being significantly more reduced than sEPSCs in KD mice (sIPSCs: −71.42 ± 3.91%; sEPSCs: −42.42 ± 4.89%; n = 17 cells; P = 0.0002, U = 35, Mann-Whitney test). These effects were not a result of changes in pyramidal cell membrane properties (table S5). Furthermore, to ensure that these effects were resulting from synaptic changes per se, we recorded miniature post-synaptic currents (mPSCs) and found that mIPSCs were also more affected than mEPSCs in KD mice (mIPSCs: −61.30 ± 8.35%; mEPSCs: −39.02 ± 4.54%; n = 16 cells; P = 0.01108, U = 61, Mann-Whitney test; fig. S7). Additionally, MD induced an increase in the frequency of

sEPSCs and sIPSCs in KD mice, whereas it had no effect in WT mice, which indicates that experience-dependent plasticity of both excitatory and inhibitory synapses occurs in KD but not in WT adult mice. As excitation and inhibition influence each other through homeostatic processes (*17*), we then assessed whether the E/I balance was affected by analyzing the dynamic conductances of composite synaptic responses evoked by intracortical or thalamocortical stimulation. In both cases, we found the inhibition-excitation (I/E) ratio to be reduced in KD mice (Fig. 3, D to F), which indicates that inhibition is predominantly affected by Cx30 down-regulation. Further, as found for the sEPSC versus sIPSC data, the I/E ratio increased when plasticity was induced through MD. Together, these data suggest that experience-dependent maturation of inhibitory circuits ending the critical period requires astrocytic Cx30. To investigate this possibility, we assessed the maturity of PV interneurons, which settles visual cortex inhibition, by determining the abundance of their perineuronal nets (PNN) of extracellular matrix (ECM) proteins (*11*). We found PNN to be significantly smaller in KD mice (Fig. 3, G and H), which suggests that these cells were immature. Additionally, whereas MD also decreased PNN in WT mice, it had no further effect in KD mice, which is indicative of an occlusion. Together, these data indicate that the increased expression of Cx30 through development during the critical period is required for the timely maturation of visual cortex inhibition.

RhoA-MMP9 pathway down-regulation mediates Cx30 effect

We then sought to identify the molecular pathway through which Cx30 modulates PNN extent and maturation of PV interneurons. To this end, we performed coimmunoprecipitation experiments with biotinylated WFA lectin followed by quantitative proteomics of pulled-down proteins in the visual cortex of WT and KD mice (P50) using label-free mass spectrometry. Reactome pathway analysis of enriched or unique proteins in WT compared with KD samples indicated an enrichment of proteins associated with the Rho–guanosine triphosphatases (GTPases)–KTN1 pathway (table S3 and Fig. 4A, upper panel). Conversely, analysis of proteins unique and enriched in KD compared with WT samples revealed enrichment of the Rho-GTPases–ROCK pathway (table S3 and Fig. 4A). Besides, mass spectrometry analysis of Cx30 coimmunoprecipitates indicated interactions with Rho-GTPases signaling pathways, among which the Rho-associated protein kinase ROCK2 was significantly enriched in KD compared with WT mice (table S4 and Fig. 4A, lower panel). These results suggest a role of the Rho family of GTPases in the PNN differences between WT and KD mice. RhoA, one family member of the Rho-GTPases, plays a role in cell remodeling (*18*) through the activation of ROCKs, and its interactions with different connexins have been described in other cell types (*19*, *20*). We thus investigated the expression of RhoA–GTP (guanosine triphosphate), the active form of RhoA, using immunohistochemistry in layer 4 of the visual cortex, and we found an increase in KD mice (Fig. 4B). Additionally, whereas MD also increased RhoA-GTP in WT mice, it had no further effect in KD mice, which is indicative of an occlusion.

As the RhoA-ROCK pathway can modulate the expression of the ECM-degrading enzyme matrix metalloproteinase 9 (MMP9) (*21*, *22*), we next tested whether this signaling is involved in the Cx30 regulation of PNNs and PV interneuron maturation. To do so, we assessed MMP9 expression in layer 4 of the visual cortex and found that MMP9 levels were increased in KD mice compared with WT mice (Fig. 4C). In addition, akin to RhoA-GTP, whereas MD increased MMP9 levels in WT mice, it had no additional effect in KD mice (Fig. 4C). This suggests that activation of the RhoA-ROCK pathway leads to the degradation of PNNs through MMP9, which promotes OD plasticity. We tested this hypothesis by inhibiting the ROCK signaling pathway in vivo with fasudil (Fig. 4D). Fasudil not only functionally rescued OD plasticity in KD mice to WT levels (Fig. 4E) by restoring the WT adult pattern of visual cortex responses after MD (Fig. 4F), it also fully rescued both MMP9 levels and PNN extent in KD MD mice (Fig. 4, G and H). These data therefore indicate that astrocytic Cx30 regulates OD plasticity through the RhoA-ROCK signaling pathway controlling MMP9 levels and PV cell maturation.

In all, we demonstrate that astrocytes regulate experience-dependent plasticity in the mouse visual cortex during the critical period. We show that astrocytes achieve this through a developmental increase in Cx30 expression, which inhibits expression of MMP9 through the RhoA-ROCK pathway, thereby hindering maturation of local inhibitory neuronal circuits. Thus, astrocytes coordinate the shaping of synaptic circuits that trigger critical-period closure. Beyond its role in regulating the visual critical period, the signaling pathway identified here may also be involved in the structural synaptic plasticity associated with cognitive functions, because Cx30 regulates the structure and efficacy of the tripartite synapse in the hippocampus (*23*). The regulation of MMP9 levels that we describe occurs by means of signaling through Cx30, which regulates the wiring of brain circuits. Because extended critical periods are associated with neurodevelopmental defects resulting in sensorimotor or psychiatric disorders (*24*, *25*), our results may provide a basis for the development of strategies to reinduce a period of enhanced plasticity in adults to favor rehabilitation after brain damage or developmental malfunction.

REFERENCES AND NOTES

1. C. A. Doll, K. Broadie, *Front. Cell. Neurosci.* **8**, 30 (2014).
2. G. Dallérac, J. Zapata, N. Rouach, *Nat. Rev. Neurosci.* **19**, 729–743 (2018).
3. T. Papouin, J. Dunphy, M. Tolman, J. C. Foley, P. G. Haydon, *Phil. Trans. R. Soc. B* **372**, 20160154 (2017).
4. L. E. Clarke, B. A. Barres, *Nat. Rev. Neurosci.* **14**, 311–321 (2013).
5. D. H. Hubel, T. N. Wiesel, *J. Physiol.* **206**, 419–436 (1970).
6. K. Lehmann, S. Löwel, *PLOS ONE* **3**, e3120 (2008).
7. C. M. Müller, J. Best, *Nature* **342**, 427–430 (1989).
8. S. B. Hofer, T. D. Mrsic-Flogel, T. Bonhoeffer, M. Hübener, *Curr. Opin. Neurobiol.* **16**, 451–459 (2006).
9. J. D. Cahoy *et al.*, *J. Neurosci.* **28**, 264–278 (2008).
10. G. Ghézali *et al.*, *Development* **145**, dev155275 (2018).
11. T. Pizzorusso *et al.*, *Science* **298**, 1248–1251 (2002).
12. I. Erchova, A. Vasalauskaite, V. Longo, F. Sengpiel, *Phil. Trans. R. Soc. B* **372**, 20160159 (2017).
13. H. Y. He, B. Ray, K. Dennis, E. M. Quinlan, *Nat. Neurosci.* **10**, 1134–1136 (2007).
14. G. Di Cristo *et al.*, *Nat. Neurosci.* **10**, 1569–1577 (2007).
15. T. K. Hensch *et al.*, *Science* **282**, 1504–1508 (1998).
16. D. Tropea *et al.*, *Nat. Neurosci.* **9**, 660–668 (2006).
17. G. G. Turrigiano, S. B. Nelson, *Nat. Rev. Neurosci.* **5**, 97–107 (2004).
18. C. Gonzalez-Billault *et al.*, *Cytoskeleton* **69**, 464–485 (2012).
19. H. J. Kim *et al.*, *Int. J. Mol. Sci.* **21**, 1255 (2020).
20. A. Mendoza-Naranjo *et al.*, *PLOS ONE* **7**, e37374 (2012).
21. K. J. Jeong *et al.*, *Oncogene* **31**, 4279–4289 (2012).
22. L. Tong, V. Tergaonkar, *Biosci. Rep.* **34**, e00115 (2014).
23. U. Pannasch *et al.*, *Nat. Neurosci.* **17**, 549–558 (2014).
24. J. J. LeBlanc, M. Fagiolini, *Neural Plast.* **2011**, 921680 (2011).
25. R. M. Meredith, *Neurosci. Biobehav. Rev.* **50**, 180–188 (2015).

ACKNOWLEDGMENTS

The authors thank N. Dufour, C. Joséphine, MIRCen's viral vector facility, G. Sadoc for his help with Elphy, the animal and imaging facilities of College de France, as well as M. Roux from the mouse clinical institute for technical assistance. **Funding:** This work was supported by grants from the European Research Council (consolidator grant no. 683154), European Union's Horizon 2020 research and innovation program (Marie Sklodowska-Curie Innovative Training Networks, grant no. 722053, EU-GliaPhD), and UNADEV-Aviesan to N.R.; from Région Ile-de-France and Fondation pour la Recherche Médicale to D.L.; from College de France to G.D.; from Fyssen Fondation to J.Z.; and from French Research Ministry (Biosigne Doctoral school) to R.B. **Author contributions:** Conceptualization: N.R., G.D., J.R., and C.M.; Data curation: G.D., J.R., R.B., D.L., and N.R.; Formal analysis: G.D., J.R., R.B., P.B., J.Z., V.S., D,L., M.M., and N.R.; Funding acquisition: N.R. and G.D.; Investigation: J.R., R.B., G.D., C.-F.C., F.D., P.E., K.S., J. Z., and N.R.; Methodology: J.R., G.D., and J.M.; Resources: D.L. and A.-P.B.; Supervision: N.R. and G.D.; Project administration: N.R.; Validation: J.R., G.D., and N.R.; Visualization: J.R., R.B., G.D., and N.R.; Writing original draft: G.D. and N.R.; Writing – review and editing: all authors. **Competing interests:** The authors declare no competing interests. **Data and materials availability:** All data are available in the manuscript or the supplementary materials. Reasonable requests for materials sharing will be fulfilled upon completion of a material transfer agreement.

SUPPLEMENTARY MATERIALS

science.sciencemag.org/content/373/6550/77/suppl/DC1
Materials and Methods
Figs. S1 to S8
Tables S1 to S5
References (*26*–*49*)
MDAR Reproducibility Checklist

View/request a protocol for this paper from *Bio-protocol*.

1 November 2020; accepted 13 May 2021
10.1126/science.abf5273

Astrocytes close the mouse critical period for visual plasticity

Jérôme Ribot, Rachel Breton, Charles-Félix Calvo, Julien Moulard, Pascal Ezan, Jonathan Zapata, Kevin Samama, Matthieu Moreau, Alexis-Pierre Bemelmans, Valentin Sabatet, Florent Dingli, Damarys Loew, Chantal Milleret, Pierre Billuart, Glenn Dallérac and Nathalie Rouach

Science **373** (6550), 77-81.
DOI: 10.1126/science.abf5273

How astrocytes close a critical period

During the visual critical period, brain circuits are rewired to adjust to sensory input. Closure of the critical period stabilizes the circuits. Looking at development in the mouse visual cortex, Ribot *et al.* found that astrocytes increase their expression of the gap junction channel subunit connexin 30, which in turn inhibits expression of a matrix-degrading enzyme (see the Perspective by Kofuji and Araque). As the matrix stabilizes, inhibitory interneurons mature, and the unusual flexibility of the critical period comes to an end.

Science, abf5273, this issue p. 77; see also abj6745, p. 29

Science (print ISSN 0036-8075; online ISSN 1095-9203) is published by the American Association for the Advancement of Science, 1200 New York Avenue NW, Washington, DC 20005. The title *Science* is a registered trademark of AAAS.